Article:
Razali, R, Valavanis, A, Cooper, JD et al. (2016) Mid-infrared entangled photon generation in optimised asymmetric semiconductor quantum wells. Superlattices and Microstructures, 90. 107 - 116. ISSN: 0749-6036

https://doi.org/10.1016/j.spmi.2015.11.015

Mid-infrared entangled photon generation in optimised asymmetric semiconductor quantum wells

R. Razali[a,c,*], A. Valavanis[a], J. Cooper[a], Z. Ikonić[a], D. Indjin[a], P. Harrison[b]

[a] *School of Electronic and Electrical Engineering, University of Leeds, Woodhouse Lane, Leeds LS2 9JT, United Kingdom.*
[b] *Materials and Engineering Research Institute, Sheffield Hallam University, Howard Street, Sheffield, South Yorkshire S1 1WB, United Kingdom.*
[c] *Physics Department, Faculty of Science, Universiti Teknologi Malaysia, 81310, Skudai, Johor, Malaysia.*

Abstract

The optimal design of asymmetric quantum well structures for generation of entangled photons in the mid-infrared range by spontaneous parametric down-conversion is considered, and the efficiency of this process is estimated. Calculations show that a reasonably good degree of entanglement can be obtained, and that the optical interaction length required for optimal conversion is very short, in the few μm range.

Keywords: optimised quantum well, SPDC, nonlinear optics, entangled twin photons

1. Introduction

Generation of entangled photons, and of heralded single photons, is a very important ingredient in a variety of quantum information technologies. Experimental implementation of these techniques, using optics, requires a reliable source of correlated/entangled and single photons. This is usually implemented by the spontaneous parametric downconversion (SPDC) process in a nonlinear optical medium with non-zero second order susceptibility, where the pump

*Corresponding author
Email addresses: elrbr@leeds.ac.uk (R. Razali), A.Valavanis@leeds.ac.uk (A. Valavanis), z.ikonic@leeds.ac.uk (Z. Ikonić), D.Indjin@leeds.ac.uk (D. Indjin), p.harrison@shu.ac.uk (P. Harrison)

photon gets split into a 'signal' and 'idler' photon. The twin photons are usually polarisation-entangled. However, one can also use the spectral (frequency) entanglement of the photon pair.

In the visible or near-infrared wavelength range, the commonly used materials for this purpose are nonlinear optical crystals like lithium niobate, which have relatively large nonresonant nonlinear susceptibility. There are bulk materials which are good in the mid-infrared range, however at these longer wavelengths one can also take advantage of much larger resonant nonlinearities achievable in semiconductor heterostructures, based on intersubband transitions between size-quantized states therein. Second-order nonlinearity is available in asymmetric semiconductor quantum well structures. High nonlinearity appears in relatively narrow ranges of photon energies, near the transition resonances, which are typically in the mid-infrared range. In contrast to SPDC based on conventional nonlinear crystals, which enable different polarizations of signal and idler photons, and hence the polarization entanglement, a specific feature of Γ-valley intersubband transitions is that their nonlinearity exists only for light polarization perpendicular to the QW layer, hence disabling polarization entanglement. This type of SPDC is also known as type-0 parametric process. Here we consider the design of high efficiency entangled photon sources by optimizing the profile of semiconductor quantum wells so to obtain maximal second order nonlinear susceptibility, and consider the efficiency of spectrally entangled twin photon generation.

2. SPDC generation of twin photons in quantum wells

The SPDC process is illustrated in Figure 1. The photon-pair generation is a second order nonlinear process in which a pump photon with frequency ω_p is spontaneously converted into two photons with lower energy, called signal and idler photons, with frequencies ω_s and ω_i respectively. The process is allowed in materials with non-zero second order susceptibility. Generally, resonantly enhanced susceptibility in quantum wells is accompanied by a large absorption,

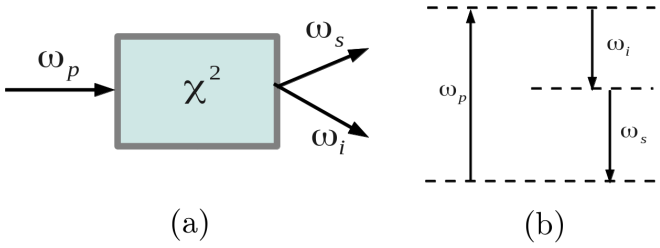

Figure 1: Spontaneous Parametric Down Conversion Process (SPDC). (a) Geometry of SPDC, (b) Energy-level diagram describing the SPDC process

which in its own right, unrelated to phase-matching issues, leads to a limited useful interaction length in such structures.

Since SPDC is a second order nonlinear process, the polarization of SPDC is defined by Eq. (1)

$$\mathbf{P} = \epsilon_0 \chi^{(2)} \mathbf{E}^2 \ . \tag{1}$$

The second-order nonlinear susceptibility ($\chi^{(2)}$) is calculated as [1, p. 174]:

$$\begin{aligned}\chi^{(2)}\left(\omega_p+\omega_q,\omega_p,\omega_q\right) = \frac{e^3 N}{2\epsilon_0 \hbar^2} \sum_{lmn} \left(\rho_{ll}^{(0)} - \rho_{mm}^{(0)}\right) d_{ln} d_{nm} d_{ml} \\ \left\{ \frac{1}{\left[\left(\omega_{nl}-\omega_p-\omega_q\right)-i\Gamma_{nl}\right]\left[\left(\omega_{ml}-\omega_p\right)-i\Gamma_{ml}\right]} \right. \\ + \frac{1}{\left[\left(\omega_{nl}-\omega_p-\omega_q\right)-i\Gamma_{nl}\right]\left[\left(\omega_{ml}-\omega_q\right)-i\Gamma_{ml}\right]} \\ + \frac{1}{\left[\left(\omega_{nm}+\omega_p+\omega_q\right)+i\Gamma_{nm}\right]\left[\left(\omega_{ml}-\omega_p\right)-i\Gamma_{ml}\right]} \\ \left. + \frac{1}{\left[\left(\omega_{nm}+\omega_p+\omega_q\right)+i\Gamma_{nm}\right]\left[\left(\omega_{ml}-\omega_q\right)-i\Gamma_{ml}\right]} \right\}\end{aligned} \tag{2}$$

where ω_p and ω_q are the input, and $\omega_p + \omega_q$ the output photon frequencies, and Γ_{ij} are the linewidths. The total electron density is N, and $N\rho_{ii}^{(0)}$ is the electron density in quantised state i. The summation over lmn in Eq. (2) goes over all states in the system. The d_{ij} in Eq. (2) is the dipole transition matrix element, and for Γ-valley intersubband transitions it has only the z-component

(perpendicular to the QW layer plane), so $\chi^{(2)}$ denotes the $\chi^{(2)}_{zzz}$ component of the susceptibility tensor.

Dipole matrix elements are calculated from the wave functions of states in the quantum well structure, obtained by solving the effective-mass Schrödinger equation. We have here used the effective-mass model with nonparabolicity, and the Schrödinger equation was solved by linearisation of the nonlinear matrix eigenvalue problem, as described in detail in [2]. In this case the d_{ij} cannot be calculated from the conventional expression $\langle\psi_i|\,\hat{z}\,|\psi_i\rangle$, as can be easily checked by varying the origin of the coordinate z (this changes the calculated values of d_{ij}, because of wavefunctions' non-orthogonality if the nonparabolicity is accounted for). Instead, the matrix elements of the momentum operator ($P_z = i\hbar\dfrac{d}{dz}$) are first calculated from [3]:

$$\langle\psi_i|\,\widehat{P}\,|\psi_j\rangle = \frac{1}{2}\,\langle\psi_i|\,P_z\frac{m_0}{m(E_i,z)} + \frac{m_0}{m(E_j,z)}P_z\,|\psi_j\rangle \tag{3a}$$

$$= \frac{i\hbar m_0}{2}\left[\int_0^\infty \psi_i\frac{d}{dz}\left(\frac{\psi_j}{m(E_i,z)}\right)dz + \int_0^\infty \psi_i\frac{1}{m(E_j,z)}\frac{d\psi_j}{dz}dz\right] \tag{3b}$$

which contains the nonparabolic (energy-dependent) effective mass. This is then recast into the conventional dipole matrix element, to be used in Eq. (2), according to:

$$\langle\psi_i|\,\widehat{z}\,|\psi_j\rangle = \frac{\hbar}{im_0}\frac{\langle\psi_i|\,\widehat{P}\,|\psi_j\rangle}{E_i - E_j}. \tag{4}$$

and this can be checked to be independent on the choice of the coordinate origin.

3. Optimization of Heterostructure for SPDC

Structural optimization for SPDC aims to find the global maximum of $\chi^{(2)}$ value, among all possible quantum well designs. These may generally include arbitrary smooth or abrupt potentials, coming from appropriate variation of the AlGaAs alloy composition, and in cases of susceptibilities relevant for the second harmonic generation, third harmonic generation, or optical rectification, has been the subject of numerous studies, based on a variety of methods. Here

we restrict considerations to the (practically most interesting) case of multiple rectangular quantum wells made of the same material (GaAs) and barriers made from another single material composition (AlGaAs). A single rectangular (hence symmetric) QW gives $\chi^{(2)} = 0$, as do all the symmetric MQWs, because the cyclic product of matrix elements in Eq.(2) is zero therein, but unequal-width double QWs (DQW), or MQWs are acceptable candidates.

Since an extensive search over the parameter space is too demanding even for the simplest, double QW structure which has the two well widths and the barrier width describing its shape, we have used a genetic algorithm to find the global maximum of $\chi^{(2)}$. This starts with an arbitrary DQW (or MQW) structure, and varies the layer widths, one at a time, initially with a large step length (50Å), in order to perform the initial 'scan' of the parameter space, and keeps twenty best structures as 'parents'. The initial width for each well and barrier is set to 2Å and the maximum width allowed is 100Å. The step length is then halved and the best structure between all daughter structures, coming from each parent, is kept. **In this calculation the daughter structures were obtained by directly mutating the parents individually, without cross-fertilization between different parents.** The search for the maximum is repeated until the step length is 1Å, which is the smallest step that can be realistically guaranteed experimentally. The method is computationally reasonably fast in finding the global maximum of $\chi^{(2)}$. **Certainly, in exceptional cases it may happen that the method finds only a local, rather than global maximum, but even then the result is practically useful.**

Table 1 shows different quantum well structures, optimised for $\chi^{(2)}$, found by this method, for different nonlinear interactions: SPDC denotes the spontaneous parametric downconversion, followed by a number which denotes the idler photon energy in meV that was used in the design. Since the meaning of signal and idler in the SPDC case is interchangable, a structure name is chosen to be consistent with Figure 1. E.g., the SPDC50 structure produces 50 meV and 150 meV photons, just as SPDC150 does, but the former has the property that the intermediate state in it is $\hbar\omega_s \approx 150$ meV from the ground

Table 1: The optimized structures with different number of QWs, for various SPDC cases - either nearly degenerate or very non-degenerate. The layer widths are given in Å, with the outermost layers being the barriers.

	Double-QW	**Triple-QW**	**Quad-QW**
SPDC99	100/27/10/61/100 $\chi^{(2)}$ =1.2879e-7	100/22/6/10/6/57/100 $\chi^{(2)}$ =1.3079e-7	100/12/5/19/10/50/2/9/100 $\chi^{(2)}$ =1.2687e-7
SPDC98	100/27/10/61/100 $\chi^{(2)}$ =1.2758e-7	100/22/6/10/6/57/100 $\chi^{(2)}$ =1.2709e-7	100/12/5/19/10/50/2/9/100 $\chi^{(2)}$ =1.2332e-7
SPDC97	100/26/10/62/100 $\chi^{(2)}$ =1.1890e-7	100/21/5/10/7/58/100 $\chi^{(2)}$ =1.2137e-7	100/12/5/19/10/50/2/9/100 $\chi^{(2)}$ =1.1784e-7
SPDC96	100/26/10/62/100 $\chi^{(2)}$ =1.1279e-7	100/58/5/11/7/20/100 $\chi^{(2)}$ =1.1438e-7	100/21/4/9/7/55/5/4/100 $\chi^{(2)}$ =1.1251e-7
SPDC67	100/20/17/60/100 $\chi^{(2)}$ =7.4714e-8	100/59/8/5/9/18/100 $\chi^{(2)}$ =7.6715e-8	100/7/2/11/9/8/9/58/100 $\chi^{(2)}$ =7.6799e-8
SPDC50	100/17/21/60/100 $\chi^{(2)}$ =7.5064e-8	100/14/11/9/15/58/100 $\chi^{(2)}$ =7.9230e-8	100/23/13/17/12/14/15/58/100 $\chi^{(2)}$ =7.6047e-8

state. **It is interesting to note that the optimisation procedure delivers the SPDC50 energy configuration as globally optimal, i.e. having a larger $\chi^{(2)}$ than that achievable in the best – but in fact only locally optimal – SPDC150 structure (the latter could be found by putting additional constraints in the optimisation procedure).** So, each entry in Table 1 corresponds to a particular nonlinear process in a particular optimised structure. All structures in Table 1 are GaAs quantum wells embedded in AlGaAs barriers with the Al concentration fixed to 48.1%. The highest $\chi^{(2)}$ value in most cases is obtained for triple QW structures, so only these are used in further discussion of SPDC entangled photon generation.

Resonantly enhanced nonlinearities are always accompanied with increased absorption, which has to be taken into account when considering the efficiency of optical processes. The absorption coefficient α, is found from the imaginary

part of the linear susceptibility ($\chi^{(1)"}$) [1, p. 167], and is calculated from:

$$\alpha = \chi^{(1)"}\omega/c \ , \tag{5}$$

with ω is the photon angular frequency, c is the speed of light and

$$\chi^{(1)"} = \sum_n \frac{e^2 N d_{ij}^2}{3\hbar\varepsilon_0}\left[\frac{\Gamma_{ij}}{\Gamma_{ij}^2 + (\omega_{ij}-\omega)^2} - \frac{\Gamma_{ij}}{\Gamma_{ij}^2 + (\omega+\omega_{ij})^2}\right] \ . \tag{6}$$

For resonant structures the absorption also peaks at pump and signal / idler photon energies.

4. Twin Photon Generation

The quantitative analysis of twin-photon generation in media which have optical losses have been presented in [4]. For non-degenerate twin-photon generation, the expression for the correlated twin (ω_1, ω_2) photon flow is [4]:

$$P_{\text{Twin}} = \frac{c|\kappa|^2 P_3 L}{|n_1 - n_2|}\frac{e^{-2\alpha_3 L} - e^{-2(\alpha_1+\alpha_2)L}}{2(\alpha_1+\alpha_2-\alpha_3)L} \ . \tag{7}$$

and in the degenerate case, where the signal and idler frequencies are (almost) the same, the corresponding expression is [4]:

$$\begin{aligned} P_{\text{Twin}} =& \frac{4|\kappa|^2 P_3 L^{3/2}}{3\sqrt{2\pi|g|}}\frac{3e^{-|\alpha_{11-3}|L}}{2|\alpha_{11-3}L|^{3/2}} \\ & \times \int_0^{\sqrt{|\alpha_{11-3}L|}} \sinh(|\alpha_{11-3}L| - x^2)\ dx \ . \end{aligned} \tag{8}$$

where $\alpha_{11-3} = \alpha_1 + \alpha_2 - \alpha_3$ (the absorption difference) and $g = [\partial^2\beta/\partial\omega^2]$, with $\beta = 2\pi n_{p/2}/\lambda_{p/2}$.

The n_i and α_i in Equation (7) and (8) are the refractive index and absorption coefficient at photon frequency ω_i, L is the length of the device, P_3 is the pump power, and κ is related to $\chi^{(2)}$ via

$$|\kappa|^2 P_3 = \sqrt{\frac{4\omega_1^2\omega_2^2 d_{\text{eff}}^2 |A_3|^2}{k_1 k_2 c^4}} \ . \tag{9}$$

where $d_{\text{eff}} = 0.5\chi^{(2)}$, and k_i is the wavenumber for photon i. A_3 is related to the intensity of the pump (a value of I_3=1 kW/cm^2 was used in calculations),

with $A_3 = \sqrt{2I_3/(\epsilon_0 c n_3)}$. The refractive indices n_i in eq. (7) depend on the photon wavelengths. These are calculated using Sellmeyer's equation for GaAs and AlGaAs [5], using the weighted average of the refractive indices for the constituent binary compounds in the structure (this is justified because the wavelengths involved are far larger than any layer thickness in the structure). The refractive index also depends on the temperature of the heterostructure [6], and in these calculations room temperature was assumed.

The structures were designed / optimised for the largest $\chi^{(2)}$ at the specified values of ω_s and ω_i, but from (7) or (8) it is clear that the actual twin photon generation rate also depends on the structure length, and on the absorption at all the involved frequencies, **and the transition linewidth will thus also indirectly influence the conversion efficiency. All this implies that the best performance may not even be necessarily obtained "at resonance". The optimal (in $\chi^{(2)}$ alone) structure profile itself is not affected by the choice of linewidth (we have checked that, and only the actual value of $\chi^{(2)}$ at resonance is affected). An alternative approach to the structure design would be to optimise for efficiency, considering the linewidth, interaction length and signal / idler frequencies as additional optimisation parameters. However, to reduce the number of parameters, in this work we have used the optimisation of $\chi^{(2)}$, and have subsequently varied the signal / idler frequencies, linewidth, and the interaction length in order to find the best performance achievable under realistic conditions.**

4.1. Non-degenerate case

Fig. 2 and 3 show the pump to twin-photon conversion efficiency for non-degenerate cases, using two different optimized structures (designed to split pump photons into two photons with the ratio of their frequencies either 2:1 or 3:1). The actual values of pump or signal photon energies were then varied around the design values, and the transition linewidth was also varied, and in each case the length which produces the largest conversion rate is found and

recorded. **This (optimal) conversion length should be well below the coherence length of the nonlinear process, otherwise a serious reduction of "effective" $\chi^{(2)}$ would take place (or some reduction if quasi-phase-matching is employed). For the pump frequency and splitting ratios considered here, using the Sellmeyer's equation again gives the coherence lengths of ∼1000–1500 μm, and the conversion length was required to be below 100 μm, but the actual values found in non-degenerate cases were much smaller than that.** The results in Fig. 2 show that a larger linewidth requires a larger interaction length for the maximum efficiency, and even then this efficiency is smaller than for narrow linewidths. Furthermore, as shown in Fig. 3, for realistic values of the linewidth (mid-range in Fig. 2) a structure may not perform best under the exact resonance conditions for which it is designed, i.e. some detuning from it may actually improve the conversion, on account of the reduced absorption, despite the simultaneous decrease of the $\chi^{(2)}$ value.

4.2. Degenerate Case

Fig. 4 shows the nearly-degenerate twin-photon conversion efficiency, Eq. (8), as it depends on the signal/idler frequency in the SPDC99 structure, calculated for a couple of different linewidths. The optimal interaction length, required for this conversion, is shown in Fig. 4(b), but is limited to 100μm, both in order to keep phase-mismatching negligible and to have a very short SPDC converter. Fig. 4(c) shows the frequency dependence of $\chi^{(2)}$ of this structure for different linewidths, this is clearly very different from the conversion efficiency, due to the influence of absorption.

5. Schmidt Number

The SPDC-generated twin-photon state can be written as [7],

$$|\Psi\rangle = A \iint dv_+ dv_- \alpha(v_+)\phi(v_-)\, |2^{-1/2}(v_+ + v_-)\rangle_s\, |2^{-1/2}(v_+ - v_-)\rangle_i \ , \quad (10)$$

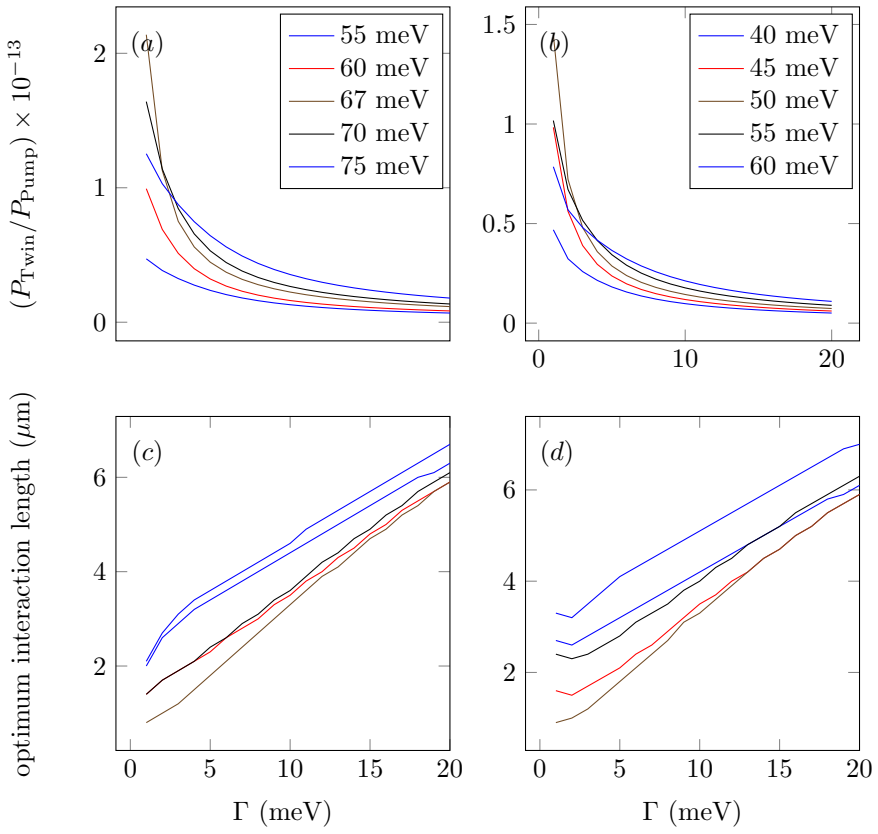

Figure 2: The pump to twin-photon conversion efficiency calculated for the optimised non-degenerate case structures for different idler's energy (coloured line). The left plot (a,c) is for the case where the structure is optimised for idler = 1/3 × pump (67 meV), and the right plot (b,d) for the structure optimised for idler = 1/4 × pump (50 meV).

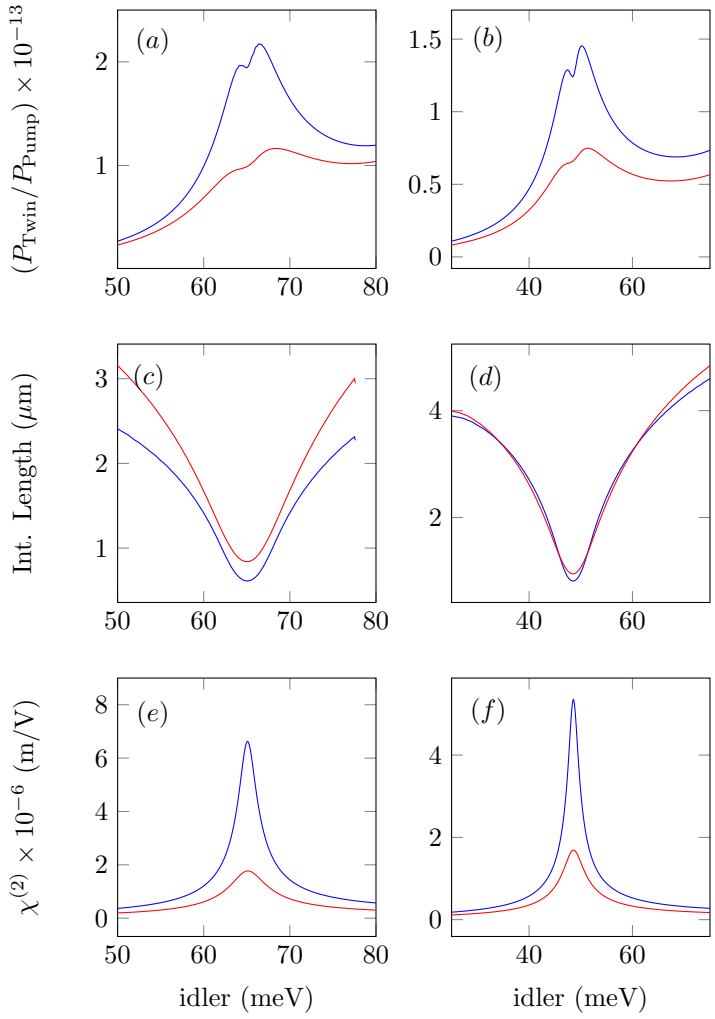

Figure 3: The pump to twin-photon conversion efficiency calculated for the optimised non-degenerate case structures, with the linewidth of 1 meV (blue line) and 2 meV (red line). The left plot (a,c,e) use the best structure for case as the idler being 1/3 of the pump energy (67 meV) and the right plot (b,d,f) is for case as the idler being 1/4 of the pump energy (50 meV).

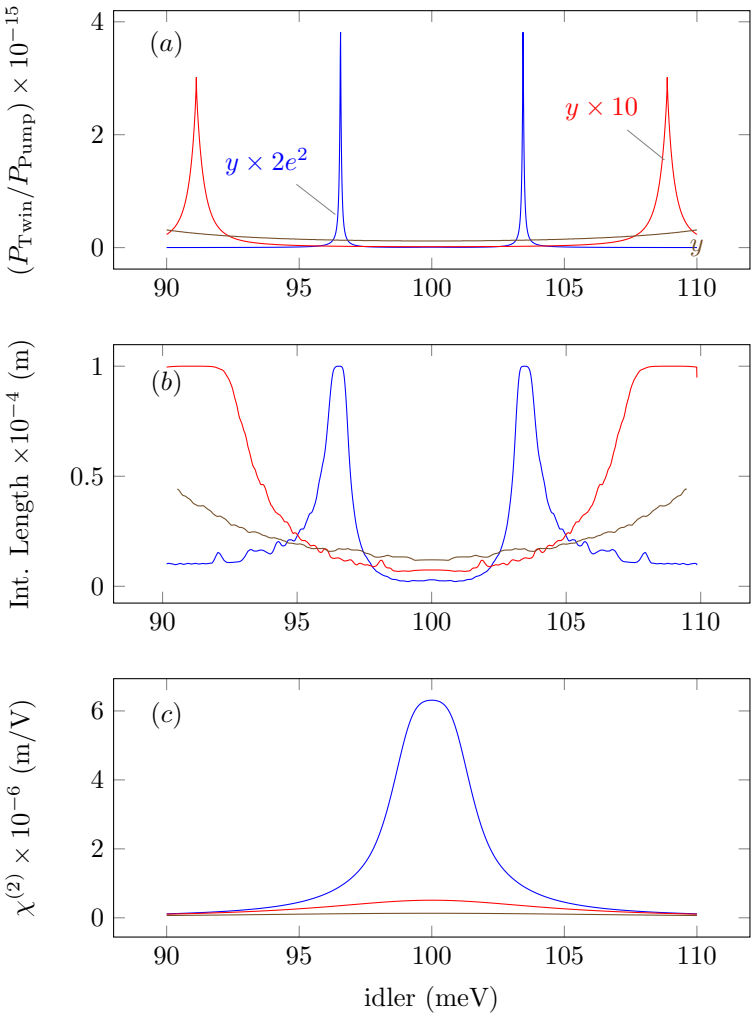

Figure 4: (a) The pump to almost-degenerate twin-photon generation efficiency of the SPDC99 structure, calculated for different linewidths, 1 meV (blue), 5 meV (red), and 10 meV (brown line); (b) the optimal interaction length, necessary for the efficiency shown in (a), and (c) $\chi^{(2)}$ in the optimised structure, for different linewidths.

where A is the normalization constant, and $|...\rangle_\mu$ (with $\mu = s, i$) represent the single photon Fock states in signal and idler modes. $\alpha(v_+)\phi(v_-)$ in Eq. (10) is the joint amplitude of pump envelope function (PEF) $\alpha(v_+)$ and 'phase-matching function' (PMF) $\phi(v_-)$, where in SPDC processes in bulk nonlinear materials the latter comes from the phase mismatch of the three waves and the presence of any quasi-phase-matching scheme applied. In the QW structures considered here the conversion lengths are very short for any significant phase mismatch to appear, but the nonlinearity is strongly resonant, i.e. dispersive.

The amount of quantum entanglement (including polarization, spatial and spectral degree of freedom) between two-photon states generated in SPDC process can be quantified by the cooperativity parameter known as Schmidt Number K. The minimum allowed value of K is 1, which corresponds to no entanglement. Based on Eq. (10), if $\alpha(v_+)$ and $\phi(v_-)$ can be approximated as Gaussian functions, with the full width at half maximum (FWHM) of σ_+ (for the pump power) and σ_- (for the twin-photon power) respectively, and if $\sigma_+ \ll \sigma_-$, the K value can be obtained from a simple analytical expression in Eq. (11) [7]:

$$K = \frac{1}{2^{1/2}} \frac{\sigma_-}{\sigma_+} \ . \tag{11}$$

The pump at these, mid-IR wavelengths is likely to be a quantum cascade laser, and typical bandwidths then are in the 550 kHz to 1.5 MHz range, e.g. [8]. By varying the signal and idler frequencies we find that $\phi(v_-)$ indeed has an approximately Gaussian shape, and its K value is given Table 2 (using a PEF bandwith of 1 MHz, i.e. $\sigma_+ = 4.239 \times 10^{-6}$ meV), which would imply a good degree of twin-photon entanglement, although not as high as predicted for SPDC process in transparent nonlinear bulk materials [7].

6. Conclusion

Optimization of quantum well structures to deliver large second-order nonlinear susceptibility $\chi^{(2)}$, useful for the frequency-entangled twin-photon generation by spontaneous parametric down-conversion, was performed using a genetic

Table 2: Schmidt number for different structures and different linewidths (Γ). Empty fields correspond to cases where the simple expression in Eq. (11) could not be used.

Γ (meV)	**OPT67**	**OPT50**	**OPT99**
1	7411	5901	8248
2	7716	5962	
5			12317
10			

algorithm. Calculations show that, for structures operating in the mid-infrared range, a reasonably good degree of entanglement can be obtained, and the required optimal conversion length is very short. Furthermore, the structures which have a large spacing between the lower two subbands are advantageous over structures where this spacing is small.

7. Acknowledgements

RR is grateful to the Ministry of Higher Education Malaysia and Universiti Teknologi Malaysia for providing financial support through the SLAB/SLAI Scholarship.

Appendix A. General $\chi^{(2)}$ Expansion Equation

$$
\begin{aligned}
\chi^{(2)}\left(\omega_2,\omega_1,\omega_0\right) =& \frac{e^3 N}{2\epsilon_0 \hbar^2}\left[\left(\rho_{11}^{(0)}-\rho_{22}^{(0)}\right) d_{13}d_{32}d_{21}\right. \\
&\times\left\{\left(\left[\left(\omega_{31}-\omega_0-\omega_1\right)-i\Gamma_{31}\right]\left[\left(\omega_{21}-\omega_0\right)-i\Gamma_{21}\right]\right)^{-1}\right. && \text{(A.1a)}\\
&+\left(\left[\left(\omega_{31}-\omega_0-\omega_1\right)-i\Gamma_{31}\right]\left[\left(\omega_{21}-\omega_1\right)-i\Gamma_{21}\right]\right)^{-1} && \text{(A.1b)}\\
&+\left(\left[\left(\omega_{32}+\omega_0+\omega_1\right)+i\Gamma_{32}\right]\left[\left(\omega_{21}-\omega_0\right)-i\Gamma_{21}\right]\right)^{-1} && \text{(A.1c)}\\
&\left.+\left(\left[\left(\omega_{32}+\omega_0+\omega_1\right)+i\Gamma_{32}\right]\left[\left(\omega_{21}-\omega_1\right)-i\Gamma_{21}\right]\right)^{-1}\right\} && \text{(A.1d)}\\
&+\left(\rho_{11}^{(0)}-\rho_{33}^{(0)}\right) d_{12}d_{23}d_{31}\\
&\times\left\{\left(\left[\left(\omega_{21}-\omega_0-\omega_1\right)-i\Gamma_{21}\right]\left[\left(\omega_{31}-\omega_0\right)-i\Gamma_{31}\right]\right)^{-1}\right. && \text{(A.1e)}\\
&+\left(\left[\left(\omega_{21}-\omega_0-\omega_1\right)-i\Gamma_{21}\right]\left[\left(\omega_{31}-\omega_1\right)-i\Gamma_{31}\right]\right)^{-1} && \text{(A.1f)}\\
&+\left(\left[\left(\omega_{23}+\omega_0+\omega_1\right)+i\Gamma_{23}\right]\left[\left(\omega_{31}-\omega_0\right)-i\Gamma_{31}\right]\right)^{-1} && \text{(A.1g)}\\
&\left.+\left(\left[\left(\omega_{23}+\omega_0+\omega_1\right)+i\Gamma_{23}\right]\left[\left(\omega_{31}-\omega_1\right)-i\Gamma_{31}\right]\right)^{-1}\right\} && \text{(A.1h)}\\
&+\left(\rho_{22}^{(0)}-\rho_{11}^{(0)}\right) d_{23}d_{31}d_{12}\\
&\times\left\{\left(\left[\left(\omega_{32}-\omega_0-\omega_1\right)-i\Gamma_{32}\right]\left[\left(\omega_{12}-\omega_0\right)-i\Gamma_{12}\right]\right)^{-1}\right. && \text{(A.1i)}\\
&+\left(\left[\left(\omega_{32}-\omega_0-\omega_1\right)-i\Gamma_{32}\right]\left[\left(\omega_{12}-\omega_1\right)-i\Gamma_{12}\right]\right)^{-1} && \text{(A.1j)}\\
&+\left(\left[\left(\omega_{31}+\omega_0+\omega_1\right)+i\Gamma_{31}\right]\left[\left(\omega_{12}-\omega_0\right)-i\Gamma_{12}\right]\right)^{-1} && \text{(A.1k)}\\
&\left.+\left(\left[\left(\omega_{31}+\omega_0+\omega_1\right)+i\Gamma_{31}\right]\left[\left(\omega_{12}-\omega_1\right)-i\Gamma_{12}\right]\right)^{-1}\right\} && \text{(A.1l)}\\
&+\left(\rho_{22}^{(0)}-\rho_{33}^{(0)}\right) d_{21}d_{13}d_{32}\\
&\times\left\{\left(\left[\left(\omega_{12}-\omega_0-\omega_1\right)-i\Gamma_{12}\right]\left[\left(\omega_{32}-\omega_0\right)-i\Gamma_{32}\right]\right)^{-1}\right. \\
& && \text{(A.1m)}\\
&+\left(\left[\left(\omega_{12}-\omega_0-\omega_1\right)-i\Gamma_{12}\right]\left[\left(\omega_{32}-\omega_1\right)-i\Gamma_{32}\right]\right)^{-1} && \text{(A.1n)}\\
&+\left(\left[\left(\omega_{13}+\omega_0+\omega_1\right)+i\Gamma_{13}\right]\left[\left(\omega_{32}-\omega_0\right)-i\Gamma_{32}\right]\right)^{-1} && \text{(A.1o)}\\
&\left.+\left(\left[\left(\omega_{13}+\omega_0+\omega_1\right)+i\Gamma_{13}\right]\left[\left(\omega_{32}-\omega_1\right)-i\Gamma_{32}\right]\right)^{-1}\right\} && \text{(A.1p)}\\
&+\left(\rho_{33}^{(0)}-\rho_{11}^{(0)}\right) d_{32}d_{21}d_{13}\\
&\times\left\{\left(\left[\left(\omega_{23}-\omega_0-\omega_1\right)-i\Gamma_{23}\right]\left[\left(\omega_{13}-\omega_0\right)-i\Gamma_{13}\right]\right)^{-1}\right. && \text{(A.1q)}
\end{aligned}
$$

$$+\left(\left[\left(\omega_{23}-\omega_0-\omega_1\right)-i\Gamma_{23}\right]\left[\left(\omega_{13}-\omega_1\right)-i\Gamma_{13}\right]\right)^{-1} \tag{A.1r}$$

$$+\left(\left[\left(\omega_{21}+\omega_0+\omega_1\right)+i\Gamma_{21}\right]\left[\left(\omega_{13}-\omega_0\right)-i\Gamma_{13}\right]\right)^{-1} \tag{A.1s}$$

$$+\left(\left[\left(\omega_{21}+\omega_0+\omega_1\right)+i\Gamma_{21}\right]\left[\left(\omega_{13}-\omega_1\right)-i\Gamma_{13}\right]\right)^{-1}\Big\} \tag{A.1t}$$

$$+\left(\rho_{33}^{(0)}-\rho_{22}^{(0)}\right)d_{31}d_{12}d_{23}$$

$$\times\Big\{\left(\left[\left(\omega_{13}-\omega_0-\omega_1\right)-i\Gamma_{13}\right]\left[\left(\omega_{23}-\omega_0\right)-i\Gamma_{23}\right]\right)^{-1} \tag{A.1u}$$

$$+\left(\left[\left(\omega_{13}-\omega_0-\omega_1\right)-i\Gamma_{13}\right]\left[\left(\omega_{23}-\omega_1\right)-i\Gamma_{23}\right]\right)^{-1} \tag{A.1v}$$

$$+\left(\left[\left(\omega_{12}+\omega_0+\omega_1\right)+i\Gamma_{12}\right]\left[\left(\omega_{23}-\omega_0\right)-i\Gamma_{23}\right]\right)^{-1} \tag{A.1w}$$

$$+\left(\left[\left(\omega_{12}+\omega_0+\omega_1\right)+i\Gamma_{12}\right]\left[\left(\omega_{23}-\omega_1\right)-i\Gamma_{23}\right]\right)^{-1}\Big\}\Big]\,. \tag{A.1x}$$

Appendix B. Sellmeyer's Equation for AlGaAs and GaAs

Eq. (B.1) and Eq. (B.2) shows the Sellmeyer's Equation for GaAs and AlGaAs respectively.

$$n(\lambda_{\mathrm{GaAs}}) = \sqrt{A + \frac{B}{1 - C^2/\lambda^2}} \ . \tag{B.1}$$

with λ_{GaAs} is the wavelength in μm, A=8.950, B=2.054, and C^2=0.390.

$$n(\lambda_{\mathrm{AlGaAs}}) = \sqrt{A_0 \left[f(x) + \frac{f(x_{s0})}{2} \left(\frac{E_0}{E_0 + \Delta_0} \right)^{\frac{3}{2}} \right] + B_0} \tag{B.2}$$

with,

$$\begin{aligned}
f(x) &= \frac{2 - \sqrt{1+x} - \sqrt{1-x}}{x^2} \ , \\
x &= \frac{hc}{\lambda E_0} \ , \\
x_{s0} &= \frac{hc}{\lambda (E_0 + \Delta_0)} \ . \\
A_0(x) &= 6.3 + 19.0x \ , \\
B_0(x) &= 9.4 - 10.2x \ , \\
E_0(x) &= 1.425 + 1.155x + 0.37x^2 \text{ eV}, \\
E_0(x) + \Delta_0(x) &= 1.765 + 1.115x + 0.37x^2 \text{ eV}.
\end{aligned}$$

In Eq. (B.2), $\lambda_{\mathrm{AlGaAs}}$ is in SI units, hc/λ in electron volt, and x is the Al fraction in $\mathrm{Al}_x\mathrm{Ga}_{1-x}\mathrm{As}$.

References

[1] R. W. Boyd, Nonlinear optics (2008).

[2] J. Cooper, A. Valavanis, Z. Ikonic, P. Harrison, J. Cunningham, Finite difference method for solving the Schrödinger equation with band nonparabolicity in mid-infrared quantum cascade lasers, *J. Appl. Phys.* 108 (2010) 113109–113109.

[3] C. Sirtori, F. Capasso, J. Faist, S. Scandolo, Nonparabolicity and a sum rule associated with bound-to-bound and bound-to-continuum intersubband transitions in quantum wells, *Phys. Rev. B* 50 (1994) 8663.

[4] T. Suhara, T. Nosaka, Quantum theory analysis of loss effects in guided nonlinear-optic twin-photon generation, *IEEE J. Quant. Electron.* 42 (2006) 777–784.

[5] S. Adachi, GaAs, AlAs, AlxGa1-xAs and : Material parameters for use in research and device applications, *J. Appl. Phys.* 58 (1985) R1–R29.

[6] T. Skauli, P. Kuo, K. Vodopyanov, T. Pinguet, O. Levi, L. Eyres, J. Harris, M. Fejer, B. Gerard, L. Becouarn, et al., Improved dispersion relations for GaAs and applications to nonlinear optics, *J. Appl. Phys.* 94 (2003) 6447–6455.

[7] L. Zhang, A. B. U'ren, R. Erdmann, K. A. O'Donnell, C. Silberhorn, K. Banaszek, I. A. Walmsley, Generation of highly entangled photon pairs for continuous variable bell inequality violation, *J. Mod. Opt.* 54 (2007) 707–719.

[8] L. Tombez, S. Schilt, J. Di Francesco, T. Führer, B. Rein, T. Walther, G. Di Domenico, D. Hofstetter, P. Thomann, Linewidth of a quantum-cascade laser assessed from its frequency noise spectrum and impact of the current driver, *App. Phys. B* 109 (2012) 407–414.